Overview of the Mars Pathfinder Mission and Assessment of Landing Site Predictions

M. P. Golombek,* R. A. Cook, T. Economou, W. M. Folkner, A. F. C. Haldemann, P. H. Kallemeyn, J. M. Knudsen, R. M. Manning, H. J. Moore, T. J. Parker, R. Rieder, J. T. Schofield, P. H. Smith, R. M. Vaughan

Chemical analyses returned by Mars Pathfinder indicate that some rocks may be high in silica, implying differentiated parent materials. Rounded pebbles and cobbles and a possible conglomerate suggest fluvial processes that imply liquid water in equilibrium with the atmosphere and thus a warmer and wetter past. The moment of inertia indicates a central metallic core of 1300 to 2000 kilometers in radius. Composite airborne dust particles appear magnetized by freeze-dried maghemite stain or cement that may have been leached from crustal materials by an active hydrologic cycle. Remote-sensing data at a scale of generally greater than ~1 kilometer and an Earth analog correctly predicted a rocky plain safe for landing and roving with a variety of rocks deposited by catastrophic floods that are relatively dust-free.

Mars Pathfinder (named the Sagan Memorial Station) landed on the surface of Mars on 4 July 1997 (Figs. 1 and 2), deployed a small rover (named Sojourner) (Fig. 3), and collected data from three scientific instruments [named Imager for Mars Pathfinder (IMP), α-proton x-ray spectrometer (APXS), and atmospheric structure investigation/meteorology package (ASI/MET)] and technology experiments (*1*). In the first month of surface operations the mission returned about 1.2 gigabits of data, which include 9669 lander and 384 rover images and about 4 million temperature, pressure, and wind measurements. The rover traversed a total of about 52 m in 114 commanded movements, performed 10 chemical analyses of rocks and soil, carried out soil mechanics and technology experiments, and explored over 100 m^2 of the martian surface.

Pathfinder used a rover, carrying a chemical analysis instrument, to characterize the rocks and soils in a landing area over hundreds of square meters on Mars, which provides a calibration point or "ground truth" for orbital remote-sensing observations (*1*, *2*). The combination of spectral imaging of the landing area by the IMP, chemical analyses by the APXS aboard the rover, and close-up imaging of colors, textures, and morphologies with the rover cameras offers the potential for identifying rocks (petrology and mineralogy). Before the Pathfinder mission, knowledge of the kinds of rocks present on Mars was based mostly on the martian meteorites (all mafic igneous rocks) and inferences from Viking data (*3*, *4*). In addition, small valley networks in heavily cratered terrain on Mars have been used to argue that the early martian environment may have been warmer and wetter (with a thicker atmosphere), at which time liquid water may have been stable (*5*).

The Ares Vallis landing site (Fig. 4) was selected because it appeared acceptably safe and offered the prospect of analyzing a variety of rock types expected to be deposited by catastrophic floods, which enable addressing first-order scientific questions such as differentiation of the crust, the development of weathering products, and the nature of the early martian environment and its subsequent evolution (*2*). In the selection of the Pathfinder landing site, engineering constraints were identified, surface environments and safety considerations were developed (for the robust lander), and the potential science return at different sites was considered. Sites (100 km by 200 km target ellipses) were considered safe if they were below 0 km elevation, were free of obvious hazards (high-relief surface features) in high-resolution (<50 m/pixel) Viking orbiter images, and had acceptable reflectivity and roughness at radar wavelengths, high thermal inertia, moderate rock abundance, low red-to-violet ratio, and low albedo. In selecting the Ares Vallis site using the remotely sensed data and the geologic setting, we made a number of predictions of the surface characteristics of the site (*2*), which are examined below.

Launch, cruise, entry, descent, and landing. The spacecraft was launched on 4 December 1996 and had a 7-month cruise to Mars, with four trajectory-correction maneuvers. The vehicle entered the atmosphere directly after cruise stage separa-

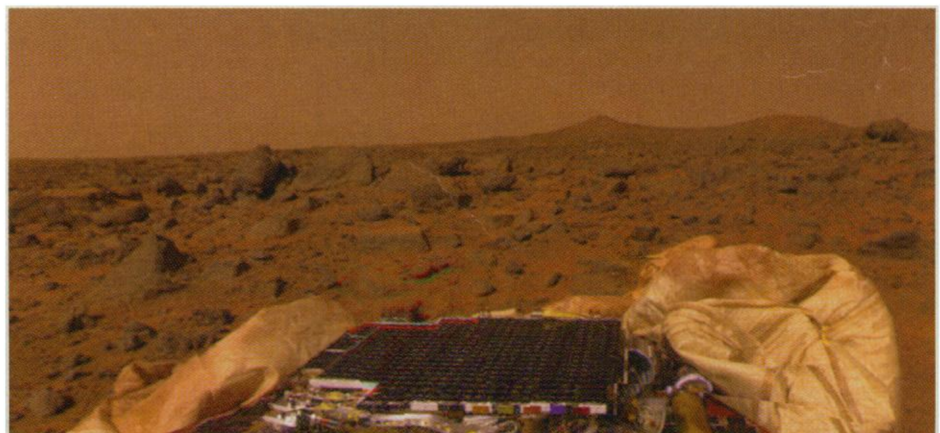

Fig. 1. Panorama of the martian surface with dark rocks, red dust, and pale pink sky at Ares Vallis taken by the IMP on sol 1; the rover is still stowed on the lander petal. Airbags inhibited deployment of the rover ramps (the gold, silver-edged cylinders at either end of the rover), and required the petal to be raised and the airbags to be further retracted, before rover egress on sol 2. Twin Peaks in the background is about 1 km to the west-southwest and contributed to rapid location of the lander in Viking orbiter images. Color mosaic is made of 24:1 compressed red filter and 48:1 green and blue filter images.

M. P. Golombek, R. A. Cook, W. M. Folkner, A. F. C. Haldemann, P. H. Kallemeyn, R. M. Manning, T. J. Parker, J. T. Schofield, R. M. Vaughan, Jet Propulsion Laboratory, California Institute of Technology, Pasadena, CA 91109, USA.
T. Economou, University of Chicago, Enrico Fermi Institute, Chicago, IL 60637, USA.
J. M. Knudsen, Niels Bohr Institute, University of Copenhagen, Denmark.
H. J. Moore, U.S. Geological Survey, Scientist Emeritus, Astrogeology Team, Menlo Park, CA 94025, USA.
R. Rieder, Max Planck Insitute for Chemistry, Mainz, Germany.
P. H. Smith, Lunar and Planetary Laboratory, University of Arizona, Tucson, AZ 85721, USA.

*To whom correspondence should be addressed.

tion. Parachute deployment, heatshield and lander separation, radar ground acquisition, airbag inflation, and rocket ignition (Table 1) all occurred before landing at 2:58 a.m. true local solar time [9:56:55 a.m. Pacific Daylight Time (PDT)]. The lander bounced at least 15 times up to 12 m high without airbag rupture, demonstrating the robustness of this landing system. The radio signal from the low-gain antenna was received at 11:34 a.m. PDT, indicating successful landing through petal opening (Table 1). During entry, descent, and landing, science and engineering accelerometers, pressure, and descent temperature sensors allowed the atmospheric temperature, pressure, and density to be reconstructed (6).

Soils near the lander that had been disturbed by retraction of the airbags appear to be a darker red-brown than the surrounding undisturbed soils (Plate 1A). Similar patches can also be found up to 15 m away from the lander to the east and southwest. Those to the southwest resemble airbag retraction marks, lie along an arc centered on the rover petal (Plate 1A), and appear to indicate that the airbag-enclosed lander rolled gently up and back down a slight rise (see azimuths 210° to 270°, elevation to 15° in Plate 1A). Dark patches extending away from the lander are probably the spacecraft's last few bounce marks as the lander bounced to its present location from the east or east-southeast (see azimuths 90° to 130°, elevations 10° to 25° in Plate 1A). These marks are distinct from the roll marks and airbag retraction marks in that they are separate patches rather than continuous swaths. Those closest to the lander (see azimuth 70°, elevation 35° in Plate 1A) also show sharp, linear troughs that fade toward the edge of the disturbed patch. These may be impressions of creases in the airbags that were imprinted into the soil as the lander bounced and compressed the airbag lobe in contact with the ground.

Surface operations. After receiving data indicating a properly functioning spacecraft, commands were sent to unlatch the IMP and high-gain antenna. Images returned at 4:30 p.m. PDT included a panorama to determine how well the airbags had been retracted, stereo images of both ends of the rover petal to determine if it was safe to deploy the rover ramps, and a partial color panorama of the martian surface and sky beyond the rover (Fig. 1). After further retraction of the airbags, which required the rover petal to be partially closed and then reopened, the ramps were deployed and the rover was commanded to stand up. A full panorama of the surface around the lander was returned during the last downlink of the first sol (the first martian day, 24.6 hours, of surface operations). The rover was driven down the rear ramp on sol 2. After acquisition of a number of lossless panoramas, the IMP was deployed on its 0.8-m-high mast at the end of sol 2. After some communication difficulties between the rover and lander on sols 1 and 2, the rover placed the APXS against Barnacle Bill on sol 3 (see rock names in Plate 6).

Operations during the first 7 sols focused on returning a full stereo lossy (compressed 6:1) panorama to support rover operations and end-of-day images of the rover to allow traverse planning for the next sol. A full three-color lossy (compressed 6:1) panorama was acquired on sol 10 and a nearly

Fig. 2. Image of lander on Mars taken from rover left front camera on sol 33. The IMP (on the lattice mast) is looking at the rover. Airbags are prominent, and the meteorology mast is shown to the right. Lowermost rock is Ender, with Hassock behind it and Yogi (Plate 6) on the other side of the lander.

Table 1. Entry, descent, and landing events.

Event	Time	Altitude	Velocity
Cruise stage separation	L - 35 min		
Entry	L - 5 min	130 km	7470 m/s
Parachute deployment	L - 134 s	9.4 km	370 m/s, 16*g*
Heatshield separation	L - 114 s		
Lander separation	L - 94 s		
Radar ground acquisition	L - 28.7 s	1.6 km	68 m/s
Airbag inflation	L - 10.1 s	355 m	
Rocket ignition	L - 6.1 s	98 m	61.2 m/s
Bridle cut	L - 3.8 s	21.5 m	
Landing	2:58 a.m.	0	14 m/s, 19*g*
Roll stop	L + 2 min		
Deflation	L + 20 min		
Airbag retracted	L + 74 min		
Petals opened	L + 87 min		

lossless three-color stereo with nine-color filter panorama was begun on sol 13. This panorama and images acquired for subpixel scale resolution represent the complete set of images for characterizing the landing site. The rover was sent in a clockwise traverse around the lander (Plate 3) to enable APXS measurements of rocks in the Rock Garden, which could not be accessed from the other direction.

Location of the lander. Five prominent features on the horizon, including three knobs, one large crater, and two small craters, were identified in lander images and in the high-resolution Viking orbiter images (Fig. 5), which allows the lander to be located with respect to other surface features. On the basis of azimuths to the features, the location of the lander in the Viking images can be determined to within a few pixels (about 100 m). Within the U.S. Geological Survey (USGS) cartographic network (*7*), the lander is located at 19.17°N, 33.21°W, but a revised cartographic network (*8*) for the local area and the two-way ranging and Doppler tracking (*9*) results in inertial space suggest that the USGS network is displaced about 19 km to the north and 7 km to the west (Figs. 4 and 5).

Geology and geomorphology. Many characteristics of the landing site are consistent with its being shaped and deposited by the Ares and Tiu catastrophic floods (*10*). The rocky surface is consistent with its being a depositional plain (16% of the area is covered by rocks; Plates 5, 8, 9, and 10) with rounded to semirounded pebbles, cobbles, and boulders that appear similar to those of depositional plains in terrestrial catastrophic floods (see below). The Twin Peaks appear to be streamlined hills in lander images, which is consistent with interpretations of Viking orbiter images of the region that suggest the lander is on the flank of a broad, gentle ridge trending northeast from Twin Peaks (Fig. 5). This ridge, which is the rise to the north of the lander, is aligned in the downstream direction from the Ares and Tiu Valles floods and may be a debris tail deposited in the wake of the Twin Peaks. Rocks in the Rock Garden (Shark, Half Dome, and Moe; Plate 6) may be imbricated blocks generally tilted in the direction of flow (Fig. 1). Channels visible throughout the scene (Fig. 1 and Plates 1b and 4) may be a result of late-stage

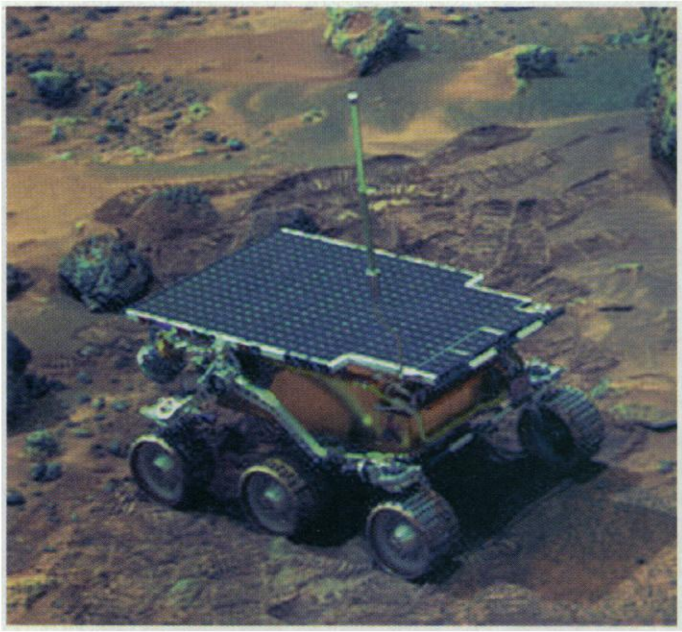

Fig. 3. Lander image of rover near The Dice (three small rocks behind the rover) and Yogi (Plate 6) on sol 22. Color (red, green, and blue filters at 6:1 compression) image shows dark rocks, bright red dust, dark red soil exposed in rover tracks, and dark (black) soil. The APXS is in view at the rear of the vehicle, and the forward stereo cameras and laser light stripers are in shadow just below the front edge of the solar panel.

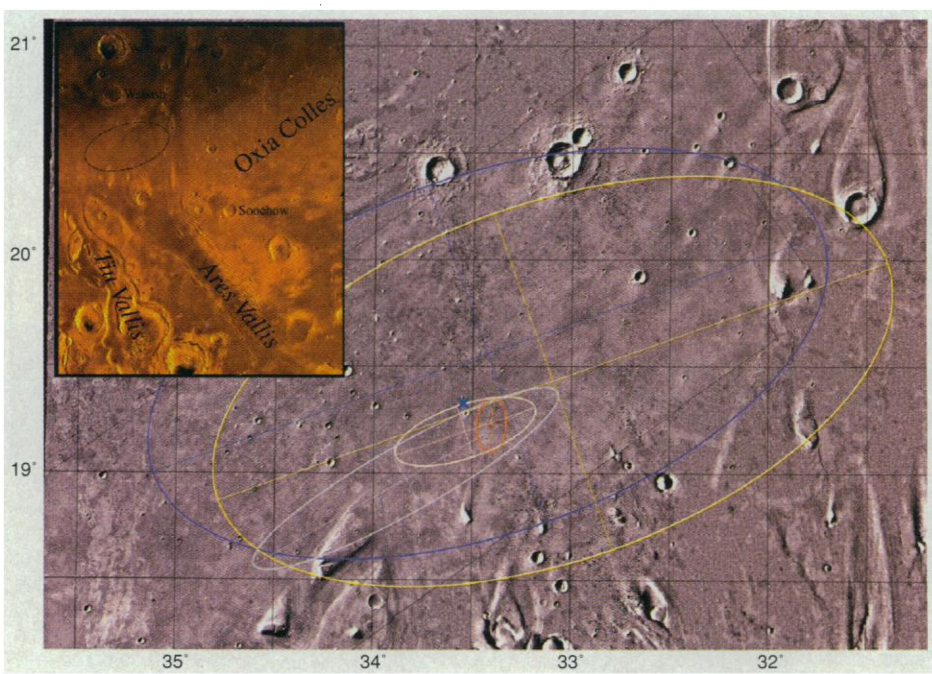

Fig. 4. Mosaic of Ares Vallis showing different landing ellipses, with color inset of the Chryse Planitia region of Mars showing the outflow channels. The large blue ellipse (100 km by 200 km) to the northwest is an ellipse in the USGS cartographic reference frame (*7*) designed to avoid streamlined hills to the south and east, craters to the north, and etched terrain to the west (this ellipse is shown in the color inset). The large yellow ellipse (100 km by 200 km) displaced toward the southeast (by 20 km in longitude and 8 km in latitude) is the navigation target ellipse in the revised local cartographic reference frame [which are the latitude and longitude shown in this figure (*8*)]. The elongate light blue ellipse (98 km by 19 km) is the navigation prediction as of late 3 July and early 4 July; it includes part of the streamlined island in the southwest. The gold ellipse (15 km by 8 km) is the prediction with tracking through atmospheric entry. The pink ellipse (41 km by 15 km), which encloses the smallest ellipse (and the location of the lander), is the navigation result with dispersions added for atmospheric entry and descent. The blue X is the location of the lander with respect to surface features identified in Viking orbiter images [located at 19.33°N, 33.55°W in the local reference frame of (*8*)]. The location of the lander in inertial space (19.30°N, 33.52°W) from the two-way ranging and Doppler tracking of the lander (*9*) is at the very northwest edge of the crater, just 2.2 km to the south-southeast of the X. If the location of the lander in inertial space is forced to coincide with its location with respect to surface features, then the resulting cartographic frame is actually 2 km to the south and 0.8 km to the east of the local network. Color mosaic is part of the Oxia Palus Quadrangle (MC 11) of Mars; black and white mosaic from Viking orbiter images of 38 m/pixel resolution; north is at the top.

drainage. Large rocks (>0.5 m) appear tabular and semirounded, and many appear perched, consistent with deposition by a flood. Smaller (<0.3 m), angular, darker rocks and blocks may be ejecta from a nearby crater (*10*). Evidence for eolian activity at the site includes wind tails behind rocks and wind streaks of what appears to be very fine-grained bright red drift material, similar in color to dust in the atmosphere. The presence of dirt covering the lower 5 to 7 cm of several rocks suggests that they have been exhumed (*10*). Some rocks appear to be fluted and grooved by saltating sand-sized particles in the wind, and light-colored sand dunes have been imaged in the trough behind the Rock Garden by the rover.

Mineralogy and geochemistry. In general, rocks are dark gray with discontinuous coatings of bright red dust or weathered surfaces, or both (*10*). Undisturbed dark soil, which appears dark (black) in surface images (Fig. 3), and dark red soil, which appears in areas disrupted by the rover and airbags, have colorations between the bright red and dark gray. A very bright red material (for example, Scooby Doo) may be an indurated soil, because its composition is similar to that of soils elsewhere at the site (*11*). Soil compositions are generally similar to those measured at the Viking sites, which are on opposite hemispheres. Thus, this soil may be a globally deposited unit on Mars (*11*). The similarity in compositions among the soils implies that the differences in color may be due to slight differences in iron mineralogy or differences in particle size and shape.

The analyzed rocks are consistent with basaltic to andesitic parent materials on Mars (*11*). The high silica content of some of the rocks appears to require crustal differentiation of mantle-derived parent materials. These rocks have compositions that are distinct from those of the martian meteorites. Analyses of rocks with lower silica content appear rich in sulfur, implying that they are covered with dust or weathered. Rover images show that some rocks appear vesiculated and may be volcanic. Soils cannot have formed from the measured rocks at the landing site because their compositions are chemically distinct (*11*).

Magnetic properties and surface material properties. Airborne magnetic dust has been progressively deposited with time on most of the magnetic targets on the lander (*12*). The dust is bright red and has a magnetization consistent with that of composite particles with a small amount of maghemite as stain or cement. Interpretation of these results suggests that the iron was dissolved out of crustal materials in water, suggesting an active hydrologic cycle on Mars, and the maghemite is a freeze-dried precipitate (*12*).

Observations of wheel tracks and soil mechanics experiments suggest that compressible, drift, cloddy, and indurated surface materials are present (*13*). Bright red drift material and others may be very fine-grained materials (dust); most are composed of poorly sorted dust, sand-sized particles, lumps of soil, and small rocks. Angles of repose and internal friction are like those on Earth and imply bulk densities of surface materials between 1.2 and 2 g/cm^3. Rover images show a large number of loose spherically rounded pebbles and cobbles on the surface. One rock in front of Shark (Plate 6) shows reflective hemispheric pockets or indentations and rounded pebbles, implying that the rock may be a conglomerate (*13*). Conglomerates require running water to smooth and round the pebbles and cobbles and to deposit the materials, and argues for a warmer and wetter past in which liquid water was stable and the atmosphere was thicker.

Atmosphere. The atmospheric opacity has been about 0.5 since landing on Mars (*10*), in late northern summer (L_s 143°). Slightly higher opacity at night and early in the morning may be due to clouds, which have been imaged, and fog. The sky has been a pale pink color (Fig. 1), similar to what was seen by the Viking landers (*14*). Particle size (roughly a micrometer) and shape and water vapor (about 10 precipitable micrometers) in the atmosphere are also consistent with measurements made by Viking (*14*). The upper atmosphere (above 60 km altitude) was relatively cold, although this may be consistent with seasonal variations and entry at 3 a.m. local solar time

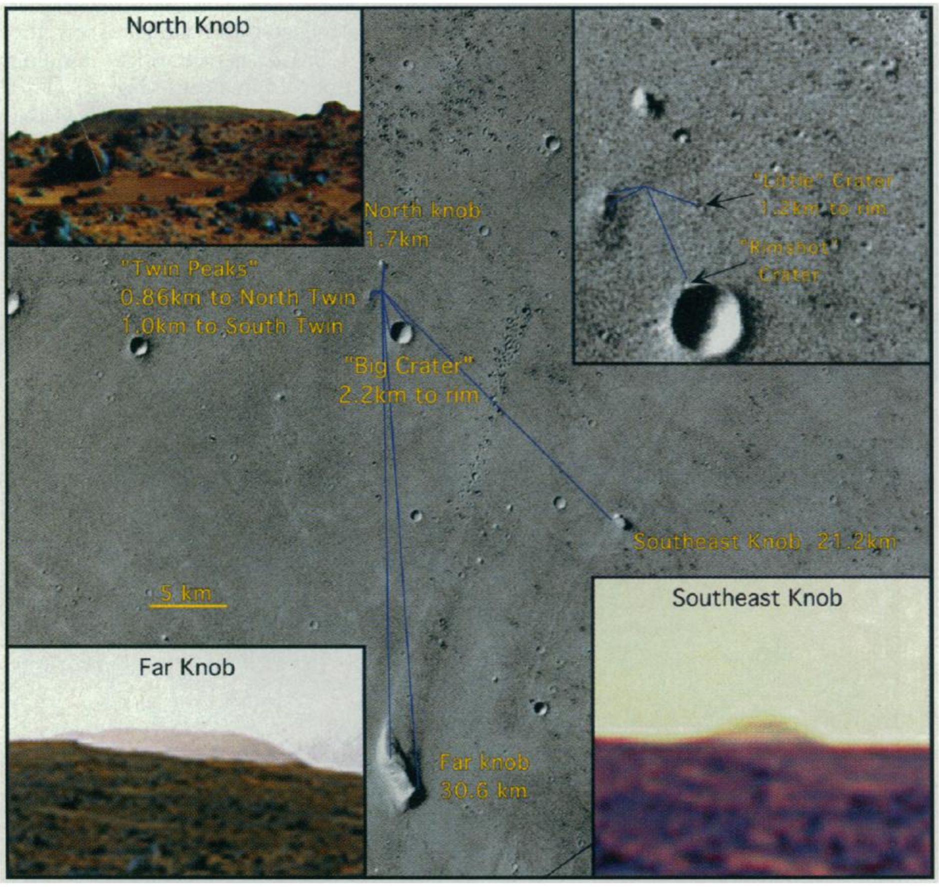

Fig. 5. Mosaic of Viking orbiter images illustrating the location of the lander (19.17°N, 33.21°W in the USGS reference frame) with respect to surface features. Five prominent features on the horizon include North Knob, Southeast Knob, Far Knob, Twin Peaks, and Big Crater. Two small craters visible in the orbiter and lander views—Little Crater and Rimshot Crater—lie on the northwest outer flank of the rim of Big Crater. Because the lander is on the southeast-facing flank of a low ridge, very distant features to the south and east are in view, whereas relatively nearby features to the north are partially or completely obscured. Only the tip of North Knob, which appears larger in the Viking orbiter images than the Twin Peaks, projects above the local horizon, and a 300-m crater, 1.2 km to the northeast, is completely obscured. Viking stereo images 004A27 and 004A87 and 004A44 and 004A70. North is up; scale bar, 5 km. (**Insets**) (**Upper right**) Lander location. (**Upper left**) North Knob from lander. (**Lower left**) Far Knob from lander. (**Lower right**) Southeast Knob from lander. The location of the lander in inertial space (19.30°N, 33.52°W) from the two-way ranging and Doppler tracking of the lander (*9*) is coincident with Rimshot Crater. Twin Peaks can be seen in Fig. 1.

[compared with the warmer upper atmosphere measured by Viking 1 at 4 p.m. local solar time (*15*)]. The multiple peaks in the landed pressure measurements and the entry and descent data are indicative of dust uniformly mixed in a warm lower atmosphere, again similar to that measured by Viking 1 (*6*, *16*).

The meteorology measurements show repeatable diurnal and higher-order pressure and temperature fluctuations (*6*). The barometric minimum was reached at the site on sol 13, indicating the maximum extent of the winter south polar cap. Temperatures fluctuated abruptly with time and between 0.25 and 1 m height in the morning. These observations suggest that cold morning air was warmed by the surface and convected upward in small eddies. Afternoon temperatures, after the atmosphere has been warmed, do not show these variations. Winds have been light (<10 m/s) and variable, peaking at night and during daytime. Dust devils have been detected repeatably in the early afternoon (*6*).

Rotational and orbital dynamics. Daily Doppler tracking and less frequent two-way ranging during communication sessions between the spacecraft and Deep Space Network antennas have resulted in a solution for the location of the lander in inertial space and the direction of the Mars rotational axis (*9*). Combined with earlier results from the Viking landers, this gives a factor of 3 improvement in the Mars precession constant. The estimated precession rate is consistent with the hypothesis that the nonhydrostatic component of the polar moment of inertia (0.3653 ± 0.0056) is due to the Tharsis bulge (*9*). The estimated precession constant rules out warm interior models with mantle compositions similar to that of Earth and cold, highly iron-enriched models. If the (iron-enriched) Shergotite meteorites are typical of the mantle composition, then the mantle must be warmer than Earth's (for the same pressure level) and the core radius must be larger than ~1300 km (but no larger than ~2000 km for other mantle compositions).

Tests of predictions for the landing site. Pathfinder has provided tests of the validity of remote observations from Earth, orbit, and the surface (*2*). As predicted, the average elevation of the center of the site was about the same as that of the Viking 1 lander (VL-1) relative to the 6.1-mbar geoid (Table 2), based on delay-Doppler radar measurements (*17*) and tracking results (*18*); the Doppler tracking and two-way ranging estimate for the elevation of the spacecraft (*9*) is only 45 m lower than that of the VL-1 and within 100 m of that expected, which is within the uncertainties of the measurements. After landing, surface pressures and winds (5 to 10 m/s) were similar to expectations based on Viking data, although temperatures were about 10 K warmer (*6*). The temperature profile below 50 km was also about 20 K warmer. As a result, predicted densities were 5% higher near the surface and up to 40% lower at 50 km, but within the entry, descent, and landing design margins. The populations of craters and small hills and the slopes of the hills measured in high-resolution (38 m/pixel) Viking orbiter images and the radar-derived slopes of the landing site are all consistent with observations of these properties in the lander images (Table 2).

A rocky surface was expected from Viking infrared thermal mapper (IRTM) observations and comparisons with the Viking landing sites (*19*–*21*). The observed cumulative fraction of area covered by rocks with diameters greater than 3 cm (Plate 9) and heights (Plate 10) greater than 0.5 m (potentially hazardous to landing) at Ares is similar (Table 2) to that predicted by IRTM observations and models of the Viking lander's rock size–frequency distributions (*2*, *22*). The IRTM prediction postulated an effective thermal inertia of 30 [10^{-3} cgs units (cal cm^{-3} s$^{-0.5}$ K^{-1})] for the rock population (*19*), but we obtain a slightly different effective thermal inertia for the rock population.

The validity of interpretations of radar echoes before landing is supported by a simple radar echo model (*23*, *24*), an estimate of the reflectivity of the soil from its bulk density (*2*, *25*, *26*), and the fraction of

Table 2. Assessment of landing site predictions.

	Landing site* predictions (*2*)	Pathfinder observations
	Elevation† (km)	
R_p (*H*)	DTM: 3389.4 (−2.0) Radar: **3389.652 ± 0.1 (−1.695 ± 0.1)**	Tracking: 3389.73 ± 0.05 (−1.62 ± 0.05)
	Atmospheric conditions‡	Within design margins
Temperature	137 K at *h* = 50 km 185 K at *h* = 0 km (*35*)	163 K at *h* = 50 km 200 K at *h* = 0 km (*6*)
Density	6.6 × 10^{-5} kg m^{-3} at *h* = 50 km 2.0 × 10^{-2} kg m^{-3} at *h* = 0 km (*35*)	40% lower at *h* = 50 km 5% higher at *h* = 0 km
Surface winds	5 to 10 m/s	5 to 10 m/s
	Site characteristics	
Crater coverage	1.2% of ellipse	Three craters visible (diameters: 1.5, 0.15, and 0.14 km)
Topographic slopes	Small hills: 10° to 25° Large hills: >20°	Twin peaks: 14° to 27° Far, Southeast, and North knobs: >30°
Local slopes§	3.5-cm delay-Doppler radar: 4.8° ± 1.3° 3.5-cm CW radar: 6.4° ± 0.6° 12.6-cm radar: 5° to 7°	Preliminary stereo measurements consistent with 5°
Radar properties	3.5-cm delay-Doppler normal reflectivity‖: 0.06 ± 0.02 3.5-cm CW quasispecular cross section‖: 0.045 3.5 cm CW diffuse cross section: 0.055 12.6 cm: 0.07–0.14	Quasispecular cross section‖: 0.05 (estimate from soil density and area, and rms slope) Diffuse cross section: 0.07 (estimate from rock abundance, reflectivity, and directivity)
Thermal inertia§	Bulk **10.4** (9.6–12.9) Fine component **8.7** (8.2 ± 0.4)	Assuming bulk 10.4 with rock abundance implies fine component 8.4
Rock abundance	Percent area from IRTM thermal spectral differencing: **18%** (average: 20.4 ± 2.1%, range: 18 to 25%) Percent area from rock size–frequency distribution models: Rocks >0.5 m high: 0.7 to 3.0%	Percent area in 3 to 6 m annulus around lander: average: 16%, range: 10 to 25% Rocks >0.5 m high: 1.5% (Yogi#)
Color	Albedo: **0.24** (0.19–0.24) Red reflectivity: 0.17–0.18 Violet reflectivity: 0.06–0.07 Red/violet ratio: 2.4 ± 0.3	Preliminary assessment indicates abundant dark gray rocks, with less dust or weathering (or both) than the Viking sites *

*Boldface values in this column refer to the pixel containing lander; other values are averages for the whole landing ellipse (100 km by 200 km). †R_p is the planet radius from the center of mass, and *H* is the elevation relative to 6.1-mbar datum. Results for Mars 50th order and degree geoid (36) indicate that Pathfinder is 17 m lower than Viking 1 lander. ‡*h* is the height above surface. §Slopes are reported as a root-mean-square (rms) angle from horizontal for a sampling of slopes with lengths <10 m. ‖For small rms slopes, normal reflectivity and quasispecular cross section are nearly equal. ¶Thermal inertia units are 10^{-3} calories cm^{-2} s$^{-0.5}$ K^{-1}. #This number is likely an overestimate based on evaluation of rocks in the far-field.

area covered by rocks (Table 2). In the calculations, the soil produces the quasispecular echo and the rocks produce the diffuse echo. The derived quasispecular cross section is comparable to the cross sections and reflectivities reported for 3.5-cm wavelength observations (Table 2). The model yields a diffuse echo that is slightly larger than the polarized diffuse echo reported for 3.5-cm wavelength observations. At 12.5-cm wavelength, similar rock populations at Ares and the VL-1 site were expected because the diffuse echoes are comparable (*27*), but the large normal reflectivities suggest that bulk densities of the soils at depth are greater than those at the surface. We also obtain a fine-component inertia near 8.4, which agrees with the fine-component inertia of 8.7 (in 10^{-3} cgs units) estimated from thermal observations from orbit by the IRTM (*28*); for this estimate, we used a bulk thermal inertia of 10.4 for the landing site (*29*), an effective thermal inertia near 40 (10^{-3} cgs units) for the rock population (*30*), and a graphical representation of Kieffer's model (*31*).

Color and albedo data for Ares suggested surfaces of materials at Ares Vallis would be relatively dust-free or unweathered before landing (*2*) compared with the materials at the Viking landing sites. This suggestion is supported by the abundance of relatively dark-gray rocks at Ares and their relative rarity at the Viking landing sites, where rocks are commonly coated with bright red dust (*32*). Finally, the 40-km-long Ephrata Fan of the Channeled Scabland in Washington state, which was deposited where channelized water flowing down the Grand Coulee filled the Quincy Basin, was suggested as an analog for the landing site (*33*) because the overall geology and geomorphology of the landing site, as interpreted from orbital images before landing, are compatible with such a depositional plain (*2*). The geology and geomorphology of the landing site (discussed earlier) is similar to such a depositional plain, and the abundance and size of pebbles, cobbles, and boulders is consistent with the expected general decrease in clast size from the mouth of the channel (*2*, *34*).

Perspective. Taken together, the rounded pebbles and cobbles and the possible conglomerate, the abundant sand- and dust-sized particles and models for their origin, and the high-silica rocks all appear consistent with a water-rich planet that may be more Earth-like than previously recognized, with a warmer and wetter past in which liquid water was stable and the atmosphere was thicker.

The prediction of the characteristics of the site for safe landing and roving indicates that remote sensing data at scales of kilometers to tens of kilometers can be used to infer surface properties at a scale of meters. The prediction that the site would be a plain deposited by a catastrophic flood is consistent with what was found at the surface and implies that some geologic processes observed in orbiter data can be used to infer surface characteristics where those processes dominate over other processes affecting the martian surface layer (*20*). Analyses of rock chemistry and close-up rover images suggest that a variety of rock types are present, consistent with the landing site being a mixture of materials from a variety of sources deposited by a flood (*2*).

Mars Pathfinder has demonstrated a robust landing design for rocky areas and other terrains on Mars. The landing site is among the rockiest parts of Mars [rockier than all but ~10% of the planet at a scale of 100 km in IRTM (*19*)], and the airbag-encased lander protected the lander through multiple bounces without damage. Even in rocky areas of Mars, small rovers are excellent for placing instruments up against rocks and imaging their textures and fabrics up close. The Pathfinder landing system and its rover are suitable for the exploration of the wide variety of terrains and surface materials of Mars.

REFERENCES AND NOTES

1. M. P. Golombek, *J. Geophys. Res.* **102**, 3953 (1997).
2. ——, R. A. Cook, H. J. Moore, T. J. Parker, *ibid.*, p. 3967.
3. H. Y. McSween, *Rev. Geophys.* **23**, 391 (1985).
4. J. Longhi, E. Knittle, J. R. Holloway, H. Wanke, in *Mars*, H. H. Kieffer, B. M. Jakosky, C. W. Snyder, M. S. Matthews, Eds. (Univ. of Arizona Press, Phoenix, 1992), pp. 184–208.
5. V. R. Baker, M. H. Carr, V. C. Gulick, C. R. Williams, M. S. Marley, in *ibid.*, pp. 493–522.
6. J. T. Schofield *et al.*, *Science* **278**, 1752 (1997).
7. E. Howington-Kraus, R. L. Kirk, B. Redding, L. A. Soderblom, in *Mars Pathfinder Landing Site Workshop II: Characteristics of the Ares Vallis Region and Field Trips in the Channeled Scabland*, M. P. Golombek, K. S. Edgett, J. W. Rice Jr., Eds. (Lunar and Planetary Institute, Houston, TX, 1995), part 2, p. 38.
8. T. C. Duxbury, in *ibid.*, pp. 35–36.
9. W. M. Folkner *et al.*, *Science* **278**, 1748 (1997).
10. P. H. Smith *et al.*, *ibid.*, p. 1757.
11. R. Rieder *et al.*, *ibid.*, p. 1770.
12. S. F. Hviid *et al.*, *ibid.*, p. 1767.
13. Rover Team, *ibid.*, p. 1764.
14. J. B. Pollack *et al.*, *J. Geophys. Res.* **82**, 4479 (1977); J. B. Pollack *et al.*, *ibid.* **84**, 2929 (1979); C. B. Farmer, D. W. Davies, A. L. Howard, D. D. LaPorte, P. E. Doms, *ibid.* **82**, 4225 (1977); R. A. Kahn, T. Z. Martin, R. W. Zurek, S. W. Lee, in (*4*), pp. 1017–1053; B. M. Jakosky and R. M. Haberle, in *ibid.*, pp. 969–1016.
15. A. Seiff and D. B. Kirk, *J. Geophys. Res.* **82**, 4364 (1977).
16. R. W. Zurek *et al.*, in (*4*), pp. 835–933.
17. A. F. C. Haldemann, D. L. Mitchell, R. F. Jurgens, M. A. Slade, D. O. Muhleman, *J. Geophys. Res.* **102**, 4097 (1997).
18. C. F. Yoder and E. M. Standish, *ibid.* **102**, 4065 (1997).
19. P. R. Christensen, *Icarus* **68**, 217 (1986).
20. —— and H. J. Moore, in (*4*), pp. 686–727.
21. H. J. Moore and J. M. Keller, *Rep. Planet. Geol. Geophys. Prog. 1990*, *NASA TM 4300* (1991), p. 160.
22. M. Golombek and D. Rapp, *J. Geophys. Res.* **102**, 4117 (1997).
23. J. V. Evans and T. Hagfors, *Icarus* **3**, 151 (1964). The model of Evans and Hagfors relates the total cross section of the polarized echo (σ_{oc}) to the quasispecular component ($\sigma^{Q}{}_{oc}$) and the diffuse component ($\sigma^{D}{}_{oc}$): $\sigma_{oc} = \sigma^{Q}{}_{oc} + \sigma^{D}{}_{oc}$. The quasispecular component ($\sigma^{Q}{}_{oc}$) is related to the normal reflectivity (ρ_o), the root-mean-square slope in radians (Θ_r), a number near unity, and the area (X) producing the quasispecular echo. The diffuse component is related to the reflectivity of the wavelength scatters (ρ_r), the directivity, and the fraction of area of scatterers producing the diffuse echo: $\sigma_{oc} = \rho_o (1 + n\Theta_r{}^2)X + \rho_r g(1 - X)$ where $\rho_o = 0.06$, $\Theta_r = 4.8°$, $X = 0.839$, $\rho_r = 0.23$, and $g = 2$.
24. T. W. Thompson and H. J. Moore, *Proc. Lunar Planet. Sci. Conf.* **19**, 409 (1989).
25. G. R. Olhoeft and D. W. Strangway, *Earth Planet. Sci. Lett.* **24**, 394 (1975).
26. J. K. Mitchell *et al.*, *Proc. Third Lunar Science Conf. Suppl. 3*, *Geochim. et Cosmochim. Acta* **3**, 3235 (1972).
27. J. K. Harmon, *J. Geophys. Res.* **102**, 4081 (1997).
28. P. R. Christensen, *ibid.* **87**, 9985 (1982); *ibid.* **91**, 3533 (1986). Other models by R. M. Haberle and B. M. Jakosky [*Icarus* **90**, 187 (1991)] and by J. N. Hayashi, B. M. Jakosky, and R. M. Haberle [*J. Geophys. Res.* **100**, 5277 (1995)] report slightly smaller inertias.
29. F. D. Palluconi and H. H. Kieffer, *Icarus* **45**, 415, (1981).
30. Our estimate of the effective thermal inertia is based partly on the work of B. M. Jakosky [*Icarus* **66**, 117(1986)]. We estimate the thermal inertia of the rock population by summing the products of the thermal inertias and areas for each rock and dividing by the total area covered by the rocks; rocks greater than 0.26 m have inertias near 50 (10 to 3 cgs units), and smaller ones vary as the 0.75 power of their diameter; 0.03-m rocks have inertias near 10.
31. H. H. Kieffer *et al.*, *J. Geophys. Res.* **82**, 4249 (1977).
32. E. A. Guinness, R. E. Arvidson, M. A. Dale-Bannister, R. B. Singer, E. Bruckenthal, *Proc. Lunar Planet. Sci. Conf. 17th*, *Part 2*, *J. Geophys. Res. Suppl.* **E575** (1987); L. K. Pleskot and E. D. Miner, *Icarus* **45**, 179 (1981).
33. M. P. Golombek, K. S. Edgett, J. W. Rice Jr., Eds., *Mars Pathfinder Landing Site Workshop II: Characteristics of the Ares Vallis Region and Field Trips in the Channeled Scabland* (Lunar and Planetary Institute, Houston, TX, 1995), part 1, p. 63; part 2, p. 47; J. W. Rice Jr. and K. S. Edgett, *J. Geophys. Res.* **102**, 4185 (1997); K. S. Edgett and P. R. Christensen, *ibid.*, p. 4107.
34. V. R. Baker, *Geol. Soc. Am. Spec. Pap.* 144 (1972), p. 73.; G. Komatsu and V. R. Baker, *J. Geophys. Res.* **102**, 4151 (1997).
35. D. A. Spencer and R. D. Braun, *American Astronautical Society/American Institute of Aeronautics and Astronautics Paper 95-379* (1995); D. A. Spencer, personal communication.
36. A. S. Konopliv and W. L. Sjogren, *JPL Publ. 95-5* (February 1995), p. 73.

37. The success of the Pathfinder mission resulted from the dedication of hundreds of engineers and scientists throughout the United States and in Germany and Denmark. The mission was managed, designed, built, and operated by the Mars Pathfinder Project of the Jet Propulsion Laboratory, California Institute of Technology, which is the National Aeronautics and Space Administration's lead center for planetary exploration, with selected components contracted out to industry. Comments by R. Arvidson and B. Jakosky helped improve the manuscript.

9 September 1997; accepted 7 November 1997